Circulation of the Glacial Atlantic: A Synthesis of Global and Regional Modeling

Christian Schäfer-Neth[1,2] and André Paul[3,4]

[1] SFB 313, Kiel University, Heinrich-Hecht-Platz 10, 24118 Kiel, Germany
[2] Department of Marine Chemistry, Bremen University, P.O. Box 330440, 28334 Bremen, Germany; present address
[3] SFB 261, Bremen University, P.O. Box 330440, 28334 Bremen, Germany
[4] Geosciences Research Division, Scripps Institution of Oceanography, University of California, San Diego, 9500 Gilman Drive, La Jolla, CA 92093-0244, USA; present address

Abstract: In recent years, a great wealth of new glacial sea-surface temperatures and salinities have been reconstructed from sediment core data for the intermediate to high latitudes of the North Atlantic. In the present study, the most recent sea-surface temperature and salinity data from the North Atlantic Ocean have been compiled to develop a physically consistent three-dimensional oceanographic scenario of circulation at the Last Glacial Maximum. For a hierarchy of numerical experiments, two general ocean circulation models, driven by traditional restoring boundary conditions, have been used. For the global experiments, a descendant of the Hamburg Large-Scale Geostrophic (LSG) ocean model has been employed, and regional experiments have been carried out with the Geophysical Fluid Dynamics Laboratory (GFDL) Modular Ocean Model (MOM). Both models are linked via the output of the global model, which is used for three-dimensional temperature and salinity restoring along the artificial boundaries of the regional model. This coupling of two models with coarse and fine resolutions offers a unique opportunity to exploit both basin-wide sediment core data coverage as well as the high spatial resolution provided by the cores from high northern latitudes.

Introduction

From the sedimentary record, only one parameter of (paleo-)oceanographic significance can be determined more or less directly: sea-surface temperature (SST) by means of its imprint on fossil faunal assemblages. All other parameters, such as sea-surface salinity (SSS), density, ventilation, and currents must be derived indirectly from other data, such as the oxygen isotope composition of foraminiferal shells. To some extent, these indirect calculations are ambiguous, and results must be assessed on the basis of additional information. Furthermore, sediment core data are generally sparse despite recent advances, and large undersampled regions still exist in various parts of the world ocean. Within this context, ocean circulation models are advantageous for two reasons. First, by tying a model to the known data points, it can compute some of the missing parameters. Second, model results can point out discrepancies between data reconstructed from sediment cores and/or inconsistencies of empirical relations which were used to deduce oceanographic parameters from sedimentological parameters.

Both modeling aspects are essential for the present study:

- As of this writing, the most extensively sampled time slice is the Last Glacial Maximum (LGM), 18,000 radiocarbon/21,500 calendar years before present. From the sediment cores taken all over the North Atlantic, 39 SST estimates and 133 $\delta^{18}O$ measurements have been utilized as tie points for the modeling of circulation, water-mass distribution, as well as heat and mass transport.
- For the haline forcing in these models, SSS has been computed from SST and $\delta^{18}O$ using a four-step interpolation method (see Appendix). However, the glacial relationship between these three parameters is not quite clear, and, in particular, the proportionality between

From *The Northern North Atlantic: A Changing Environment*, edited by P. Schäfer, W. Ritzrau, M. Schlüter, and J. Thiede, pp. 441–462, Springer, Berlin, 2000

$\delta^{18}O$ and SSS changes is still subject to debate (Schmidt 1998; Rohling and Bigg 1998). Ratios ranging from 1 : 1 (Vogelsang 1990; Schäfer-Neth 1998) to 1 : 2 (Duplessy et al. 1991; Sarnthein et al. this volume) have been proposed. In the recent Nordic Seas, ratios of as much as 1 : 3 have been reported (Simstich 1999). The implications of these extremes for paleoceanographic reconstruction are discussed below.

Models

The ocean model employed for the global experiments is based on the Hamburg Large-Scale Geostrophic (LSG) ocean model. For the standard run as described by Maier-Reimer et al. (1993), this ocean model was coupled to a simple thermodynamic sea-ice model and forced by monthly mean surface wind stress, monthly mean effective air temperature and annual mean sea-surface salinity. The effective air temperature was obtained by simply advecting observed surface air temperature with monthly mean wind velocity. This procedure yielded a fixed local cooling of the sea surface which may be attributed to cold air outbreaks from the continents, cold polar air flows in the wake of passing cyclones, etc. The duration of air temperature advection was a free parameter which, for present-day climate, could be tuned to yield a meridional overturning circulation of the strength observed. However, for a climate such as the LGM, this parameter would probably have to be re-tuned, which could be very difficult, if not impossible (cf. Fieg 1996). Accordingly, in the present version of the LSG ocean model, air temperature advection has been neglected.

The strength of the meridional overturning circulation in the LSG ocean model proves to be very sensitive to the temperature boundary conditions. Without air temperature advection, the formation of new North Atlantic Deep Water (NADW) is strongly reduced from approximately 22 Sv to 12 Sv, and its export to the Southern Ocean drops from approximately 16 Sv to 3 Sv, in agreement with similar findings by Maier-Reimer et al. (1993) and Fieg (1996).

In order to compensate for at least part of the reduction in NADW formation and export, the LSG ocean model has been modified in a number of ways. Most importantly, a new tracer advection scheme has been implemented. It is an adaptation of the scheme by Farrow and Stevens (1995) which solves the tracer advection problem by implementing a predictor-corrector method, with the predictor stage using only centered differences, but the corrector stage employing the QUICK scheme by Leonard (1979). In the present version of the LSG ocean model, the predictor stage is taken to be fully implicit in time.

The new tracer advection scheme is less diffusive than the former upwind scheme and less dispersive than the common centered difference scheme. As a result, a larger fraction of newly formed NADW does not upwell and recirculate in the North Atlantic, but flows across the equator into the South Atlantic. The price to be paid is a time step of 7.5 days, which is four times less than the monthly time step used by Maier-Reimer et al. (1993) and necessitates a linear interpolation of monthly mean sea-surface boundary conditions. But since this time step applies not only to the tracer equations at all depths but also to the momentum equations, the LSG ocean model as used in the present study is still very efficient without resorting to Bryan's acceleration technique (1984).

The sea-ice model has not been included. The LSG ocean model has, rather, been driven by monthly mean sea-surface temperatures, with sea-ice-covered grid cells set to the freezing point (= −1.8 °C). Further modifications to the LSG ocean model include a new convection scheme, which renders the water column completely stable after every time step (Marotzke 1991; Rahmstorf 1996), and explicit vertical diffusion. Finally depth-dependent horizontal and vertical diffusivities are employed (Bryan and Lewis 1979; Weaver and Hughes 1996). Hence

$$D_h(z) = D_{bh} + (D_{sh} - D_{bh}) \exp(-z/500\ \mathrm{m}),$$

such that the horizontal diffusivity D_h decreases from $D_{sh} = 8 \cdot 10^6$ cm^2 s^{-1} in the top layer to $D_{bh} = 4 \cdot 10^6$ cm^2 s^{-1} in the bottom layer. Furthermore,

$$D_v(z) = D^* + \frac{C_r}{\pi} \arctan\left[\lambda(z - z^*)\right],$$

where $D^* = 0.61$ cm^2 s^{-1}, $C_r = 1$ cm^2 s^{-1}, $\lambda = 1.5 \cdot 10^{-3}$ m and $z^* = 1000$ m, such that the vertical diffusivity D_v varies from approximately 0.3 cm^2 s^{-1} in the top layer to 1.1 cm^2 s^{-1} in the bottom layer.

The modified LSG ocean model has the same resolution, land-sea mask and bathymetry as the original model, except for the glacial experiments in which the Bering Strait is closed. The average horizontal resolution is 3.5°, and there are 11 vertical levels in total, increasing in thickness from 50 m near the surface to 1500 m near the bottom.

The regional model is based on the Modular Ocean Model (MOM) developed by Pacanowski et al. (1993). To remove the numerical difficulties caused by the con-

vergence of meridians towards high latitudes, the model uses a rotated spherical coordinate system, the north pole of which is shifted to 180° W / 30° N with respect to conventional geographical coordinates. Its horizontal resolution is 0.5°, vertical resolution ranges from 50 m at the surface to 1000 m at the bottom, with 17 levels at maximum. The model domain includes the Greenland-Iceland-Norwegian Seas (termed GNS hereafter) and adjacent basins (Fig. 1, right). The bottom topography is based on the ETOPO5 (1986) data set and has been modified to take glacial 100-m sea-level lowering (Fairbanks 1989) and shelf glaciation down to typically 200 m depth (CLIMAP 1981; Lehman et al. 1991; Mienert et al. 1992) into account. At the artificially closed southwestern boundaries, 5-grid-point-wide restoring zones are fed with the annual mean temperatures and salinities taken from the steady-state output of the global model (glacial experiments) or the Levitus (1982) data base (present-day runs). The implications of these closed boundaries are discussed below in conjunction with their effects on modeled currents and heat transport. Sea ice is accounted for by prescribing freezing point SST's and setting wind stress to zero over the ice-covered regions.

The global as well as the regional ocean models are fully three-dimensional prognostic tools and are governed by the so-called primitive equations (with the one exception that the nonlinear advective terms in the momentum balance are dropped in the LSG ocean model). At the surface, they are driven by restoring to either observed modern or reconstructed glacial sea-surface temperatures and salinities. Selected model parameters are given in Table 1.

Forcing Data

Three sets of experiments (see Table 2) were performed. Set 1 employed present-day forcing data sets to validate the models. For thermal forcing of sets 2 and 3 addressing the LGM, the CLIMAP sea-surface temperature data set was used, modified by newer SST reconstructions for the North Atlantic. Sea-surface salinity was calculated from SST and foraminiferal $\delta^{18}O$ under two different assumptions for the glacial relationship of salinity and water oxygen isotopes. The method is described in detail in Schäfer-Neth (1998); a brief review is given in the appendix.

For the LGM time slice the CLIMAP SST reconstruction in the North Atlantic was modified through the incorporation of newer data from Weinelt et al. (1996) and Sarnthein et al. (this volume). At least for summer, the interpolated forcing fields of the global and regional experiments (Fig. 1) show ice-free glacial Nordic Seas, with temperatures around 2–4 °C. In the case of the global model, the modified CLIMAP SST reconstruction for the North Atlantic has been merged with the original CLIMAP SST reconstruction for the world ocean. A seasonal SST cycle was constructed simply by fitting a sinusoid through the February (northern hemisphere winter) and August (northern hemisphere summer) data. This seasonal SST cycle is refined by a plausible seasonal cycle for sea-ice extent, with the extremes given by the CLIMAP sea-ice reconstructions for February and August. In the North Atlantic, the summer sea-ice extent is the same as for the regional model, while the winter sea-ice extent is considered to be equal to the algebraic mean of the two CLIMAP sea-ice reconstructions.

From the SST fields and oxygen isotope ratios measured on fossil foraminifer shells (see Schäfer-Neth 1998 for data sources and references), two glacial sea-surface salinity (SSS) distributions were computed based on two varying assumptions concerning the glacial relation of $\delta^{18}O$ and salinity changes. This relation is still not quite clear. Atmospheric General Circulation Models (Joussaume and Jouzel 1993; Hoffmann 1995) indicate a glacial $\delta^{18}O$ lowering of high-latitude precipitation by up to 10 ppt. If this lowering had affected global freshwater $\delta^{18}O$, the glacial ratio of $\delta^{18}O$: SSS changes may have been reduced to a value near 1 (Schäfer-Neth 1998). On the other hand, several studies (e.g. Duplessy et al. 1991; Sarnthein et al. this volume) suggest that the glacial $\delta^{18}O$: SSS ratio was not very different from the modern 1 : 1.8 ratio (GEOSECS 1987), perhaps locally modified. These two extreme assumptions were used to calculate the SSS fields for set 2 and 3 experiments.

As for SSS in the global model, a seasonal cycle was arrived at in the following manner: First a glacial anomaly for the northern hemisphere summer SSS was constructed by applying the method developed by Schäfer-Neth (1998) to the North Atlantic, using the SSS reconstructions by Melles (1991) for the Ross and Weddell Seas and assuming a homogeneous SSS increase by 1.08 units elsewhere in the world ocean. Then this glacial anomaly was added to the present-day SSS data which includes a full seasonal cycle (see Table 2).

As can be seen from Figures 1-3, the high-latitude forcing fields differ between the global and regional models. This is in part due to the employment of older reconstructions in the global model and newer reconstructions in the regional model (Tab. 2). The global experiments were run before the newest data were avail-

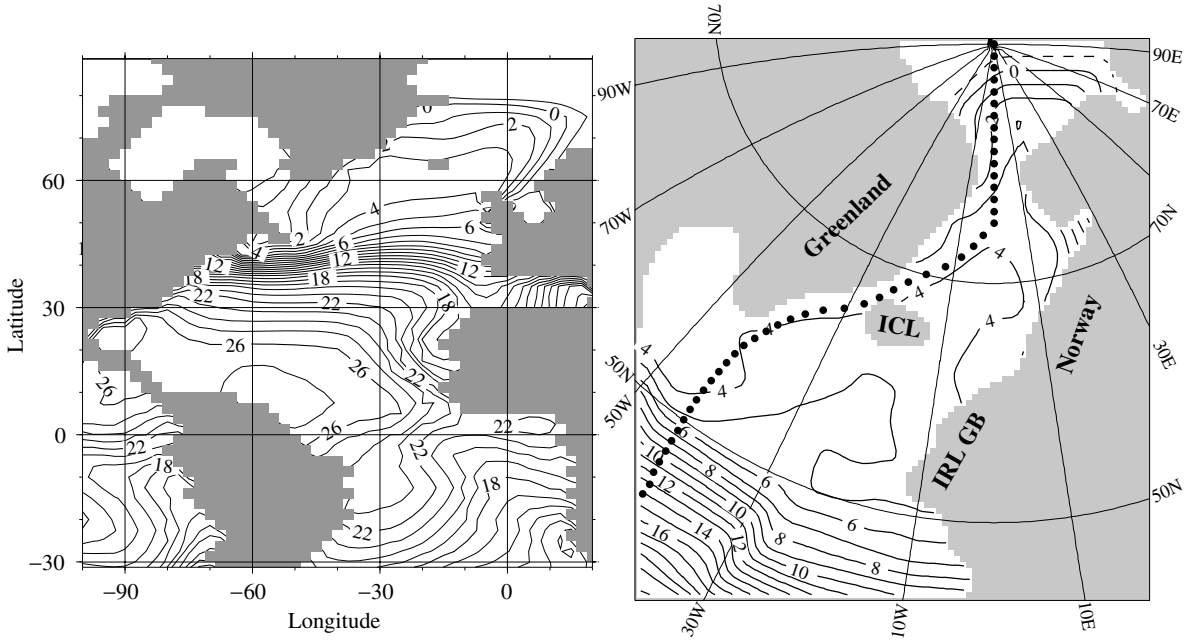

Fig. 1: Glacial summer sea-surface temperature used for forcing the global (left) and regional model (right), °C. Dots indicate the GEOSECS western Atlantic section. (The part between 74° N, the GEOSECS transect endpoint, and the North Pole is an extension of the original section.) Please note that all figures display the annual mean results from the global experiments, but the summer data from the regional experiments

Table 1: Parameters for the global and regional model

Parameter	Global	Regional
Horizontal resolution [°]	3.5×3.5	0.5×0.5
Number of levels, vertical resolution [m]	11, 50 … 1500	17, 50 … 1000
Horizontal friction [$cm^2\ s^{-1}$]	$5 \cdot 10^9$	$5 \cdot 10^8$
Vertical friction [$cm^2\ s^{-1}$]	—	1
Horizontal diffusivity [$cm^2\ s^{-1}$]	$8 \ldots 4 \cdot 10^6$	$5 \cdot 10^6$
Vertical diffusivity [$cm^2\ s^{-1}$]	0.3 … 1.1	1
Tracer time step	7.5 d	12 h
Velocity time step	7.5 d	0.5 h
Surface forcing time constant [d]	50	30
3-D restoring time constant top … bottom [d]	—	30 … 250
Integration time [a]	3600/9900	250

able. However, the differences between the two data sets are restricted to the high latitudes, which are poorly represented in the global model because of its coarse resolution and crude topography. Thus the global experiments were not rerun with the newer data; this was left for the regional model. Furthermore, the regional model was run without a seasonal cycle, because of its main purpose within the SFB 313 framework. The model served as a testing tool for SST and SSS reconstructions derived from the sediment core data as directly as possible, namely without involving a seasonal cycle taken from the present-day ocean. Because of the sparseness of core-based winter data in the GNS (cf. Sarnthein et al. this volume), this could only be done for the summer season with any geostatistical significance. The present contribution discusses the implications of this summer-only forcing.

For the regional set 2 experiments, the extreme 1 : 1-relation resulted in maximum SSS values of 35.9 in the GNS and a pronounced minimum below 35.3 in the Gulf of Biscay (Fig. 2, right). Following arguments put forth by Sarnthein et al. (this volume), the global

Table 2: Data used for surface forcing and lateral boundary restoring

Set 1 – Control runs under present-day conditions

Experiment	Global "GM"	Regional "RM"
Sea-surface T	Shea et al. 1990 [1]	Levitus 1982; Dietrich 1969 [3]
Sea-surface S	Levitus et al. 1994 [2]	
Lateral Restoring	—	
Wind	Lorenz et al. 1996	Hellerman and Rosenstein 1983 [3]

[1] SST was set to −1.8 °C over the ice-covered regions from Shea et al. (1990)
[2] Winter SSS in the Ross and Weddell Seas is adjusted according to Johns et al. (1997)
[3] SST was set to −1.9 °C and wind forcing was cut off over the ice-covered regions taken from Wadhams (1986)

Set 2 – Last Glacial Maximum with 1 : 1 relation between $\delta^{18}O$ and SSS

Experiment	Global "G1"	Regional "R1"
Sea-surface T	Weinelt et al. 1996	Sarnthein et al. this volume
Sea-surface S	via $\delta^{18}O : SSS = 1 : 1$	via $\delta^{18}O : SSS = 1 : 1$
Lateral Restoring	—	from experiment G1
Wind	Lorenz et al. 1996	Hoffmann pers. comm. 1996

Set 3 – Last Glacial Maximum with 1 : 1.8 relation between $\delta^{18}O$ and SSS

Experiment	Global "G2"	Regional "R2"
Sea-surface T	Weinelt et al. 1996	Sarnthein et al. this volume
Sea-surface S	via $\delta^{18}O : SSS = 1 : 1.8$ [4]	via $\delta^{18}O : SSS = 1 : 1.8$ (locally 2.8)
Lateral Restoring	—	from experiment G2
Wind	Lorenz et al. 1996	Hoffmann pers. comm. 1996

[4] North Atlantic Ocean only – see text

present-day ratio of 1 : 1.8 was used for set 3, and further increased to 1 : 2.8 in the GNS for the regional model experiments (Simstich 1999; after unpublished data by Erlenkeuser). This choice yields an increase of the GNS maximum to more than 36.6 and a lowering of the Biscay minimum to less than 34.4 (Fig. 3, right). The horizontal SSS gradients are approximately twice as strong in this reconstruction as in the 1 : 1 case. These regional, high-latitude SST/SSS reconstructions are assumed to be representative for the glacial summer season. They are taken as the best high-latitude glacial surface conditions available and provide the only forcing for the regional model.

In the global model, wind stress is taken from the response of the atmospheric general circulation model ECHAM 3/T42 to glacial boundary conditions, e.g., CLIMAP SST (Lorenz et al. 1996). For the regional model, the July wind stress of a glacial reconstruction obtained with the ECHAM 3/T42 atmospheric model was used, which, in turn, was run (Hoffmann 1996, pers. comm., cf. Fig. 5 in Schäfer-Neth 1998) with earlier SST reconstructions (Schulz 1994) of the ice-free glacial GNS.

Each of the experiments was integrated until a steady state was reached.

Present-Day Results

Forcing the models with present-day data sets gives quite reasonable results. In particular, the performance of the modified LSG ocean model compares favorably with that of other coarse-resolution ocean models, e.g., those based on the GFDL MOM (Danabasoglu and

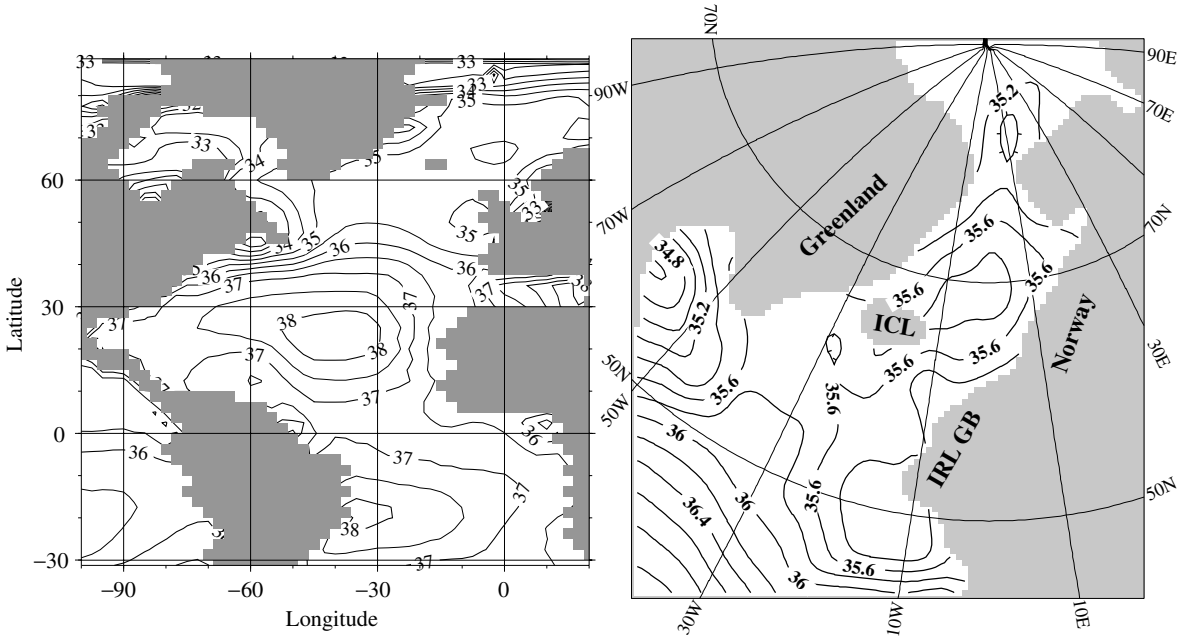

Fig. 2: Glacial summer sea-surface salinity reconstructed with a 1 : 1 relation between S and $\delta^{18}O$ changes. Left: global model, right: regional

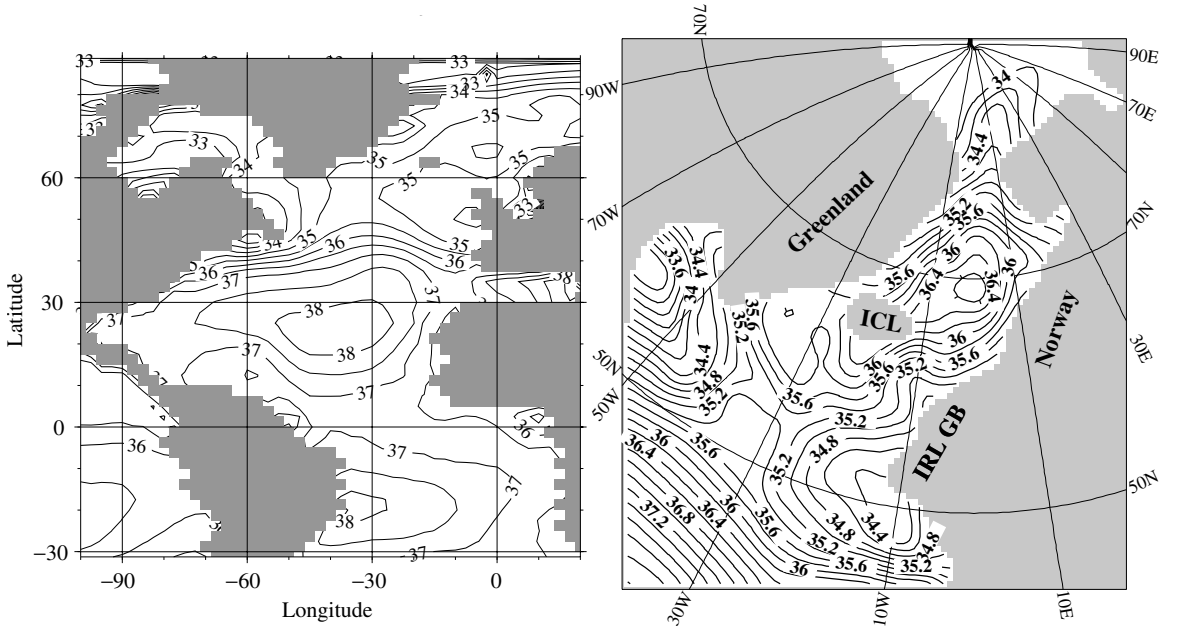

Fig. 3: Glacial summer sea-surface salinity reconstructed with a 1 : 1.8–2.8 relation between S and $\delta^{18}O$ changes. Left: global model, right: regional

McWilliams 1995; Paul et al. 1999). The horizontal circulation of the global model at 75 m and 450 m depth is depicted in Figure 4. The dominating features in the North Atlantic are the Gulf Stream and the North Atlantic Drift. A calculation of the maximum transport in the Gulf Stream yields a value of approximately 20 Sv. This value is similar to that obtained by Danabasoglu et al. (1995) and Large et al. (1997), but lower than the observed value, which is approximately 40 Sv at 30° N, upstream of the recirculation regime (Knauss 1969), or

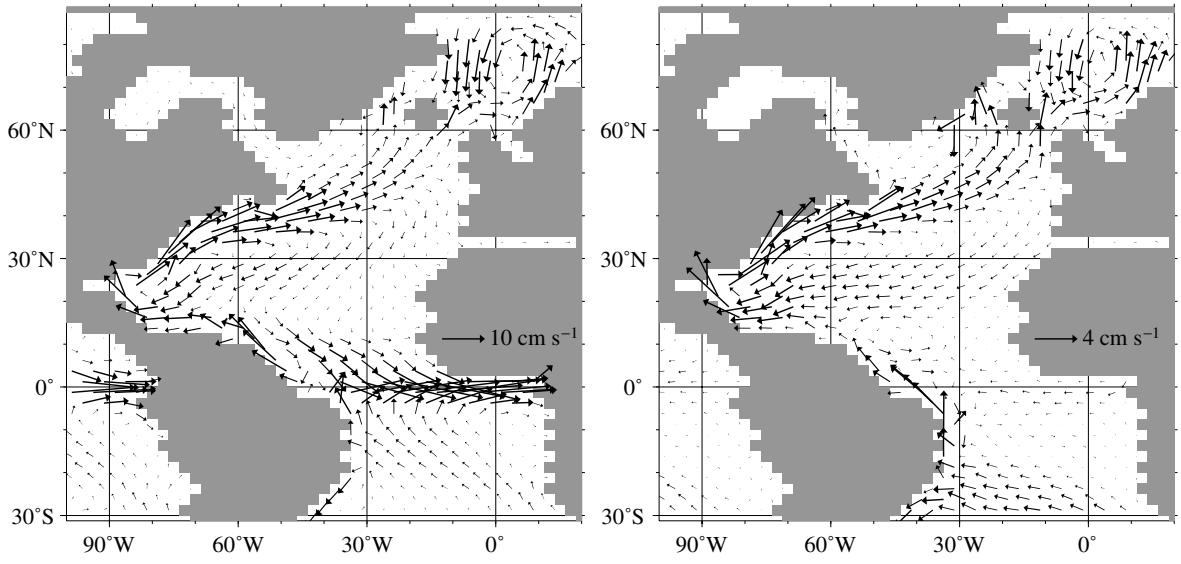

Fig. 4: Experiment GM, horizontal velocities at (left) 75 m and 450 m depth (right)

32.2 ± 3.2 Sv for the Florida Current alone (Larsen 1992). The global model reproduces the Irminger and East Greenland Currents, but generates a disproportionally strong gyre in the GNS. The representation of the circulation regime in the GNS may possibly be improved by using Dietrich (1969) temperatures and salinities for restoring, which resolve the gradients normal to the coast better than Levitus and Boyer (1994) temperatures and Levitus et al. (1994) salinities (Seidov and Prien 1996 - see also results of the regional model). In this connection it is to be noted that the sill depth of the Denmark Strait in the LSG ocean model is deeper than in the real ocean, in order to facilitate an overflow of realistic strength.

The zonally integrated meridional overturning is presented in Figure 5. "New" North Atlantic Deep Water (NADW) is produced at a rate of 14 Sv, 4 Sv of which are derived from combined overflows through the Denmark Strait and the Iceland-Faeroe-Channel, and 8 Sv of which are exported to the Southern Ocean at depths below 1500 m. There is a deep inflow of Antarctic Bottom Water (AABW) which amounts to 3–4 Sv and which is compensated by a return flow of "modified AABW" above 3500 m depth. Thus, the total amount of deep water ("pure recently formed NADW" and "modified AABW") which flows into the Southern Ocean is 11–12 Sv, approximately 40 % less than the value of 18 Sv given by Schmitz (1995).

The zonal mean boundary between the Deep Current System and the Bottom Current System is between 3500 and 4000 m deep. This depth range is close to results given by Wüst (1957). He applied the dynamic method of Bjerknes, Helland-Hansen and Sandström to 10 zonal sections of the 1925–27 "Meteor" expedition and found a circulation boundary at 3500 to 4000 m depth between 35° S and 10° N, averaged over the West Atlantic Trough, and at 3500 to 4000 m depth between 35° S and 10° S, averaged over the entire width of the Atlantic Ocean. In contrast, Macdonald (1998) com-

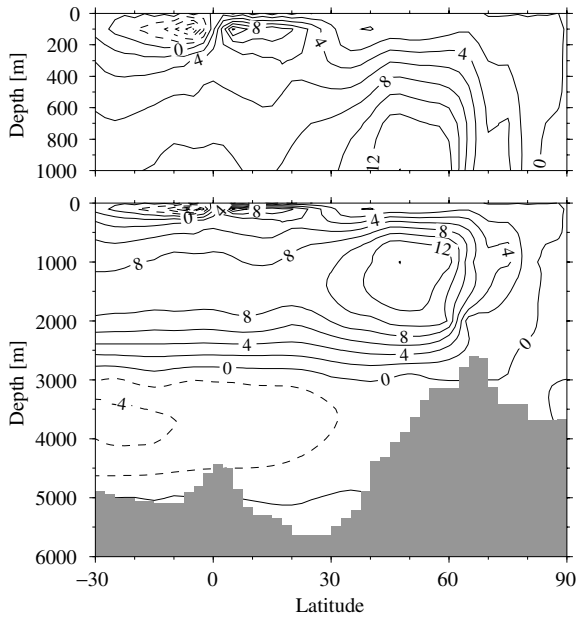

Fig. 5: Experiment GM, meridional overturning stream function, Sv

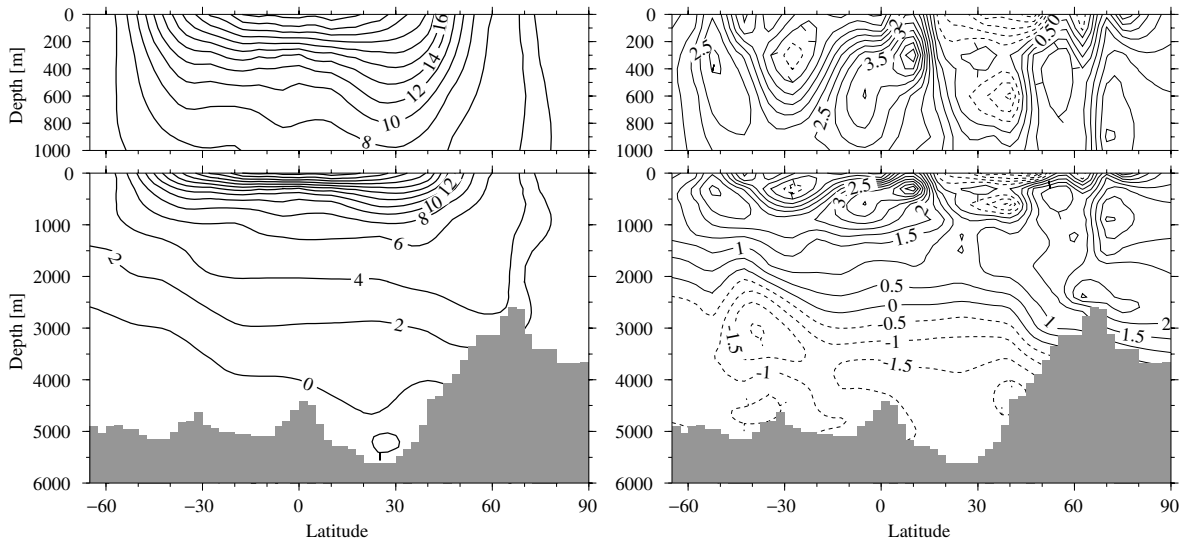

Fig. 6: Modern annual mean temperature distribution along GEOSECS transect, °C. Left: modeled (experiment GM), right: modeled minus measured

bined 15 modern high-resolution sections in a global inverse box model. In the Atlantic Ocean, she used 8 zonal sections between 27° S and 48° N. To the south of 11° N, she obtained a circulation boundary at 4000 to 5200 m depth, averaged over the entire width of the Atlantic Ocean, but to the north of 24° N, the net northward transport of bottom water in her model was not significantly different from zero.

Circulation boundaries cannot completely coincide with water-mass boundaries because of the effect of mixing, i.e., vertical turbulent transport (Wüst 1957). Figure 6 shows the temperature distribution as simulated by the global model, sampled at the GEOSECS positions and depths and compared with the GEOSECS temperature distribution on a point-by-point basis. The model thermocline is more diffuse than the observed thermocline. In the upper ocean, temperatures are therefore too warm by as much as 3.5 °C. A warm bias because of an overly diffuse thermocline is a widespread problem in coarse-resolution ocean modeling (Danabasoglu and McWilliams 1995).

AABW enters the Argentine Basin at 4000 m depth and approximately the right temperature (−0.5 to −0.6 °C), but its salinity (34.42) is too low by 0.2 units. The net export of 3–4 Sv AABW north across the equator is consistent with Schmitz (1995). Figure 6 still reveals a cold bias in the deep Atlantic Ocean of 1 to 2 °C, which indicates that the AABW is modified in its properties after upwelling in the North Atlantic Ocean and turning southward. Hence, mixing with NADW occurs only at a depth of 3000 m. The reason for this is probably that the newly formed NADW is too light to sink deep enough. In fact, according to Figure 6, temperatures above 3000 m in the northern North Atlantic Ocean are too warm by 1 to 2 °C.

In summary, the modified LSG ocean model places the depth of the circulation boundary between the Deep Current System and the Bottom Current System at 3500 to 4000 m, but yields a water-mass boundary between NADW and AABW at 2500 m depth, which is shallower by approximately 1000 m (or one layer thickness, since vertical resolution in the deep ocean is 1000 m). While the depth of the circulation boundary is roughly correct if compared to results by Wüst, the depth of the water-mass boundary is much too small. This is also born out by Figure 7, which shows that continuous mixing between AABW and NADW occurs at a depth of 3000 m rather than 4000 m or greater. Note that the temperature of the northern end member (3.64 °C) is approximately 1.5 °C too warm, and its salinity (34.75) is approximately 0.2 units too fresh, if compared to GEOSECS data (see also a similar temperature-salinity diagram by Wüst 1933).

The warm bias of the thermocline and the warm and fresh bias of deep water are both reflected in global annual mean temperature (4.18 °C) and salinity (34.58) which are approximately 0.4 °C too warm and approximately 0.2 units too fresh (see Table 3).

Validation of the regional model has been discussed in detail by Haupt et al. (1994, 1995) and Schäfer-Neth (1998). To complement these previously published results, Figure 8 displays the modeled winter circulation

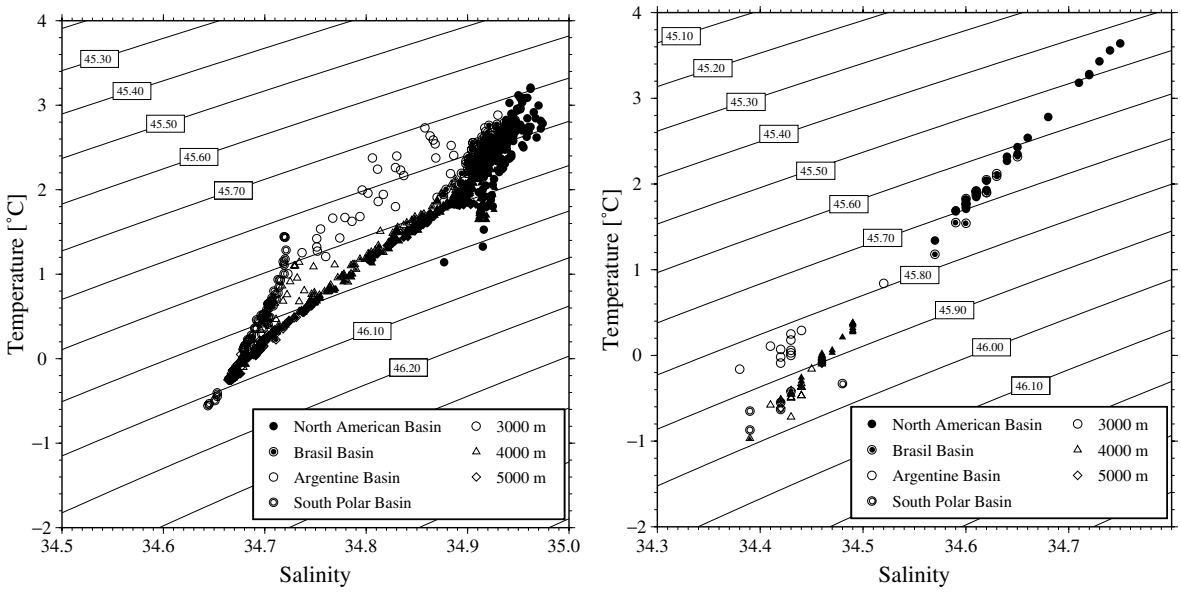

Fig. 7: Relationship between potential temperature and salinity in the Western Atlantic Trough. Left: GEOSECS data, right: experiment GM. Note that salinity ranges differ. Labeled contours are σ_4 isopycnals (i.e., potential density is referenced to 4000 db). The GEOSECS data points correspond to depth ranges 2500–3500 m, 3500–4500 m and > 4500 m. The model data points are actual grid point values and correspond to the lowest three model levels. The North American Basin corresponds to latitudes north of the equator, the Brazil Basin corresponds to latitudes between 30° S and the equator, the Argentine Basin corresponds to latitudes between 51.5° S and 30° S and the South Polar Basin corresponds to latitudes south of 51.5° S

Table 3: Annual mean temperatures and salinities of the global model. For experiment GM, the temperature anomalies ΔT and the salinity anomalies ΔS are based on the annual mean temperatures and salinities computed from the World Ocean Atlas (WOA – Levitus and Boyer 1994; Levitus et al. 1994). For experiments G1 and G2, they refer to the annual mean temperatures and salinities of experiment GM

	Global Ocean				Atlantic Ocean			
	WOA	**GM**	**G1**	**G2**	**WOA**	**GM**	**G1**	**G2**
T [°C]	3.81	4.18	2.22	2.36	4.07	4.38	2.52	2.82
ΔT [°C]		0.37	−1.96	−1.82		0.31	−1.86	−1.56
S	34.74	34.58	35.78	35.80	34.89	34.75	35.96	36.01
ΔS		−0.16	1.20	1.22		−0.14	1.21	1.26

at 75 and 450 m depth. Despite the distortion along the closed southwestern boundaries, the patterns are quite realistic in the region of main interest, namely the Nordic Seas. Fed by the North Atlantic Drift, the Norwegian Current enters the GNS, and there is an intense East Greenland Current which continues into the Labrador Current. The model even resolves small-scale features such as the Irminger Current west of Iceland. At 450 m depth, the well-known outflows from the GNS to the North Atlantic over the ridges between Greenland, Iceland and Scotland can be found. Deep convection takes place in the Norwegian Sea (down to approximately 1000 m) and the Irminger Basin (700 m) (see Sarnthein et al. this volume, Fig. 12a). In addition, the measured winter temperature distribution along the GEOSECS transect (Fig. 9, right) and a modeled section (left) have also been compared. In general, modeled distribution matches measured distribution very well, particularly in the cold, deep basins of the North Atlantic and the Nordic Seas. Exceptions are a shallower warm water sphere (T > 7 °C) south of 50° N, a deeper 4–5 °C water mass south of the Greenland-Iceland Ridge, and slightly increased temperatures in the uppermost 400 meters just north of the Ridge.

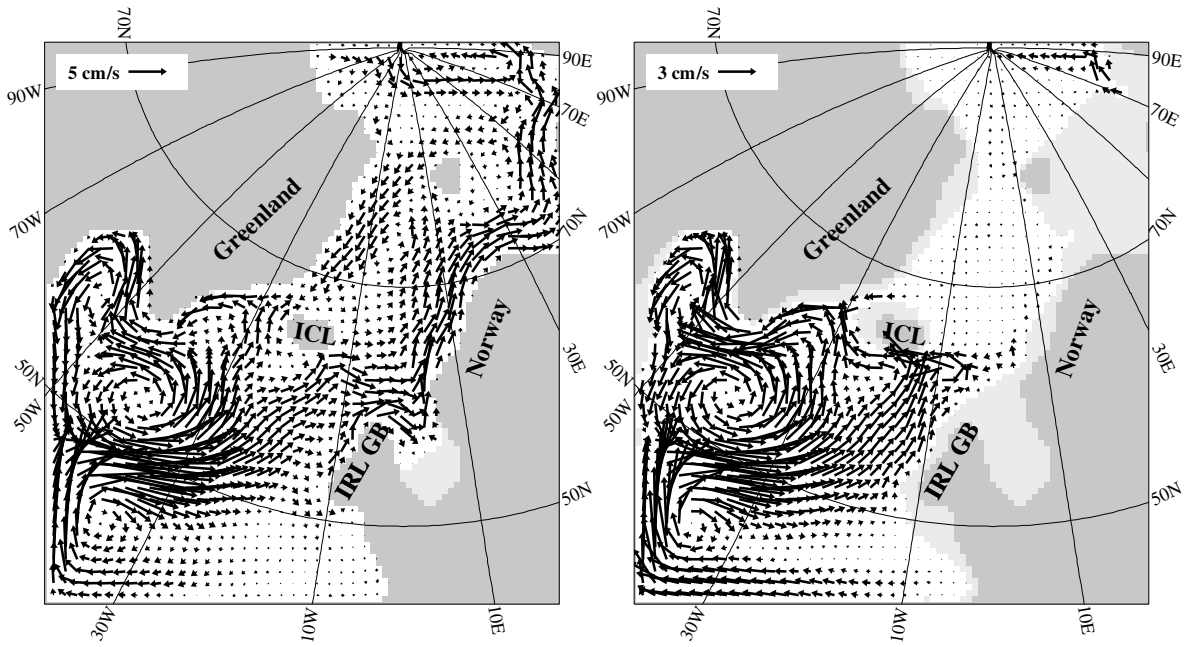

Fig. 8: Experiment RM, horizontal velocities at (left) 75 m and 450 m depth (right)

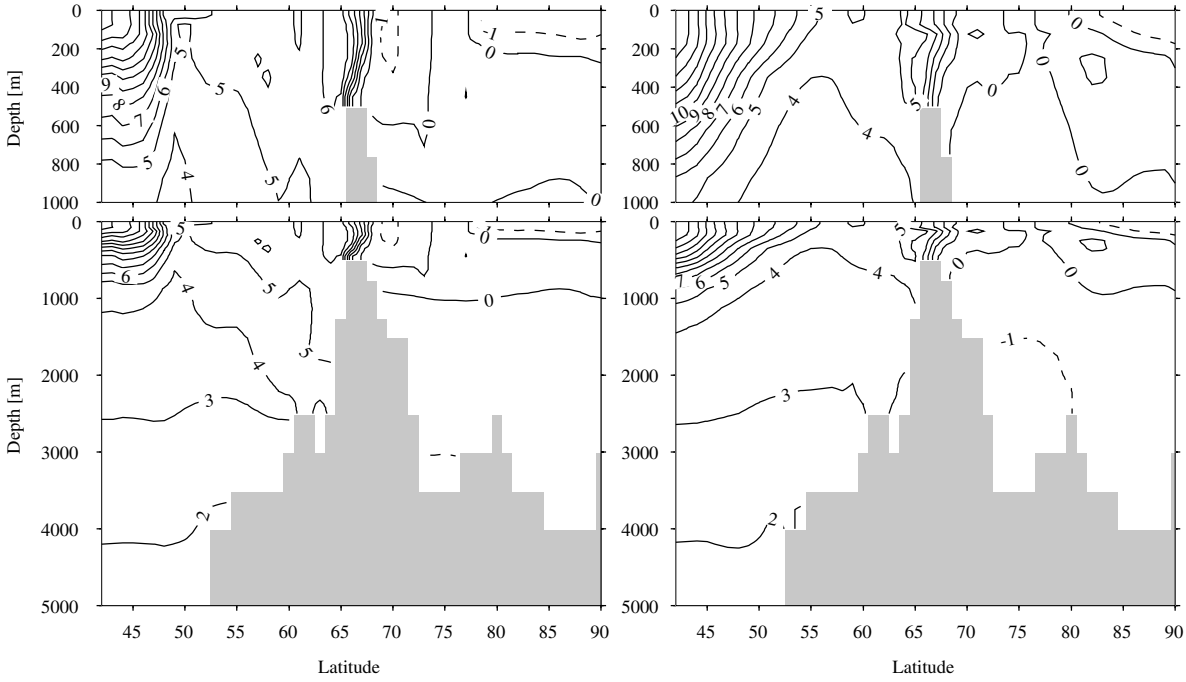

Fig. 9: Modern winter temperature distribution along GEOSECS transect, °C. Left: modeled (experiment RM), right: measured

LGM Results

In general, the two surface salinity reconstructions yield only minor differences in the global model results, which is not surprising because the different reconstructions primarily affect the high northern latitudes of the Atlantic, only a relatively small part of the global ocean. However, in the high latitudes of the regional model, the two SSS fields yield distinctly different current velocities, particularly in the GNS and at the overflows over the ridge system between Greenland and Scotland.

Horizontal Circulation Patterns

At 75 m depth in the North Atlantic (Figs. 10 and 11, left), the results of the global LGM experiments show a flow which is much more zonal and a Gulf Stream which turns more sharply eastward at approximately 45° N than in the global control experiment. The GNS gyre circulation is greatly reduced, and there is no outflow in the upper layers of the Denmark Strait. Inflow through the Denmark Strait is stronger in experiment G1 due to more intense convection. South of 30° N, experiments G1 and G2 are almost indistinguishable. With respect to experiment GM, the North Brazil Current is weakened, and the South Equatorial Current and Brazil Current are slightly stronger. At 450 m depth (Figs. 10 and 11, right), experiments G1 and G2 both exhibit a reduced westward flow at the Equator and a weakened northward, even southward, flow along the coast of northern Brazil. The recirculation in the North Atlantic is strengthened.

With respect to flow patterns, but not current velocities, both regional LGM experiments generate comparable horizontal circulation systems consisting of an upper level inflow from the North Atlantic into the GNS along the coast of Scotland (Figs. 12 and 13, left), and balancing outflows through the Denmark Strait via an intense East Greenland Current (left) and through deeper channels east of Iceland (right). This is partly in contrast to the global model results, where the flow between Greenland and Iceland heads to the northeast, quite comparable to the present-day Irminger Current, and outflows are much deeper at approximately 1000 meters or even more (not shown here). These differences can be attributed to (i) the coarser resolution of the global model and (ii) much shallower straits of the regional model. The main difference between experiments R1 and R2, caused by the varied SSS reconstruction, is an increase in current velocities from experiment R1 to experiment R2. This is due to higher SSS gradients in the 1 : 1.8–2.8-reconstruction. In the present-day ocean, overall current velocities in the northeast Atlantic and the GNS are not radically different (Fig. 8, left). In contrast to this, experiment R1 yields a marked velocity drop from the northeastern Atlantic to the GNS (Fig. 12), whereas experiment R2 inverts this north-south gradient of current velocities (Fig. 13). Additionally, experiment R2 reverses the flow direction along the coast of Ireland reverses with respect to experiment R1 and produces a relatively intense boundary current towards the Gulf of Biscay (Fig. 13, left).

According to recent glacial SST reconstructions, (Sarnthein et al. this volume, Fig. 12), inflow from the North Atlantic into the GNS reaches as far north as Svalbard. Therefore, R1 results, with drastic velocity reduction from the North Atlantic to the Norwegian Current, seem unrealistic and indicate exceptionally weak horizontal SSS gradients in the 1 : 1 reconstruction. On the other hand, an R2 velocity increase at the point where the current crosses the shallow Iceland-Scotland Ridge is highly questionable. Thus, the R2 results are to be regarded as equally unrealistic since they portray the underlying SSS gradients as too strong. Since the gradients are directly determined by the 1 : 1 and 1 : 1.8 relations used for computing SSS from SST and $\delta^{18}O$ (see Appendix 2), the "true" glacial relationship should be somewhere between these two extremes.

Meridional Mass and Heat Transports

NADW export to the Southern Ocean is reduced by 50 % and equal to 4 Sv in both global glacial experiments, although more NADW is produced in experiment G1 (Fig. 14, left) than in experiment G2 (8 Sv as compared to 6 Sv, Fig. 14, right). NADW production sites (not shown) are still located in the GNS, as opposed to glacial experiments based upon unmodified CLIMAP SST's (Fichefet and Hovine 1994; Seidov et al. 1996; Herterich et al. 1999). The wind-driven subtropical cell expands (Seidov et al. 1996). In the zonal mean, the boundary between the Deep Current System and the Bottom Current System is only very slightly shallower than in experiment GM, probably because the NADW cell is too shallow from the outset. AABW inflow still amounts to 3–4 Sv.

Changes in haline forcing result in distinctly differing overturning patterns in the regional model. With the 1 : 1 relation, the regional model extends the global model's overturning cell farther northward. There is (Fig. 15, left) a near-surface inflow into the GNS which gradually descends down to 2500 m depth at 80° N. Due to higher surface salinities, the 1 : 1.8 to 2.8

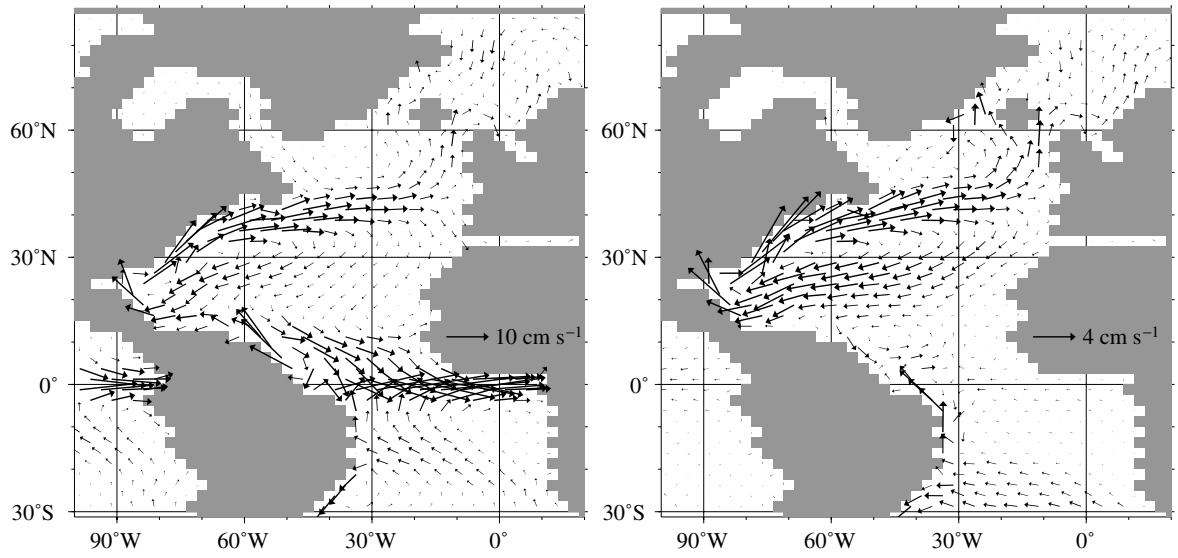

Fig. 10: Experiment G1, horizontal velocities at (left) 75 m and 450 m depth (right)

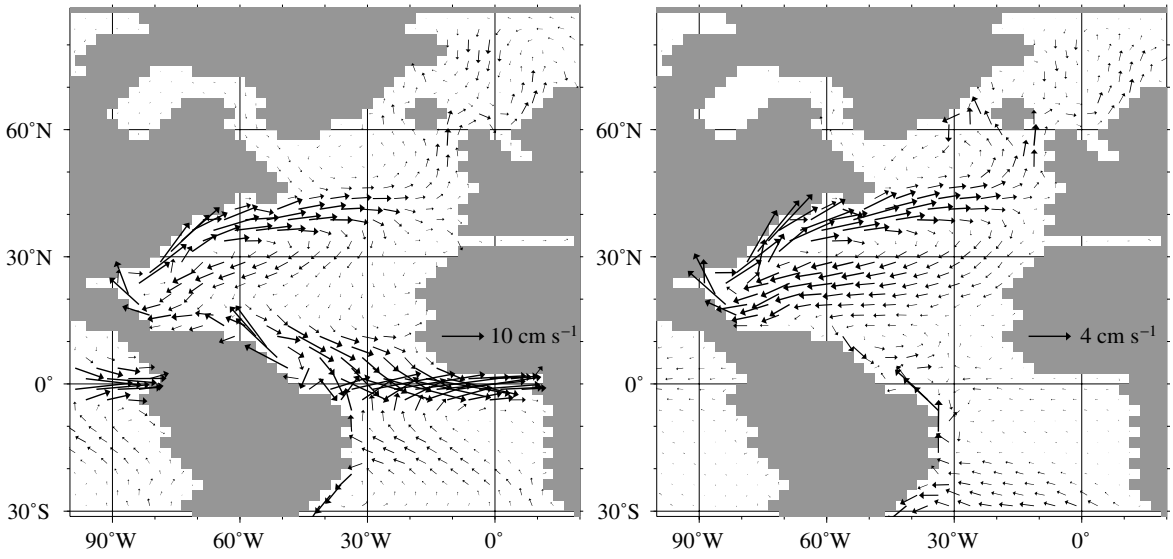

Fig. 11: Experiment G2, horizontal velocities at (left) 75 m and 450 m depth (right)

relation yields deeper and more intense convection (Fig. 21, right) in the GNS. This, in turn, results in a much stronger overturning south of 65° N (Fig. 15, right), but cuts off the northward-extending branch of the overturning cell and makes the regional results more similar to the global results.

The Atlantic's northward heat fluxes, as computed in the regional and global models, fit remarkably well (Fig. 16). In the global model, northward heat flux in the South Atlantic is reduced, in accordance with the changes in horizontal circulation patterns. The rapid drop south of 50° N in the regional experiments is caused by the artificial boundaries. Due to the higher resolution of the regional model, R1 and R2 results show small undulations associated with overflows between the North Atlantic and the GNS. Heat fluxes reach values of approximately 0.2 PW at 50° N and 0.1 PW at the latitude of the Greenland-Iceland-Scotland ridges, 62° N. The deep convection present in the regional experiments at approximately 70° N prevents any signifi-

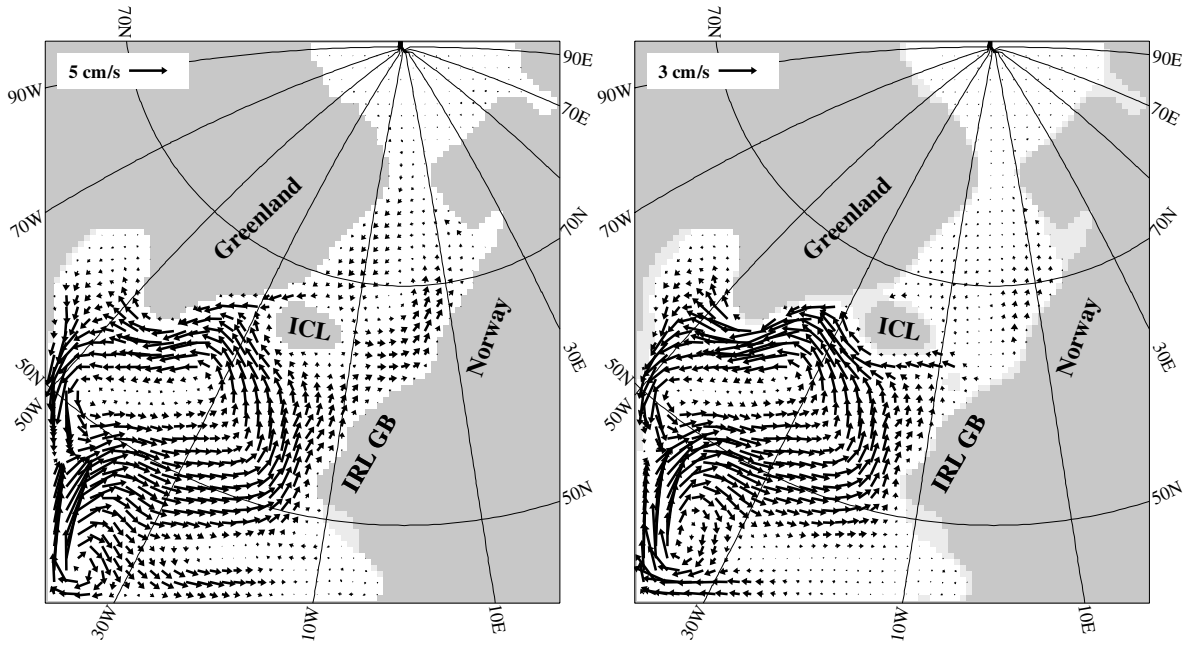

Fig. 12: Experiment R1, horizontal velocities at (left) 75 m and 450 m depth (right)

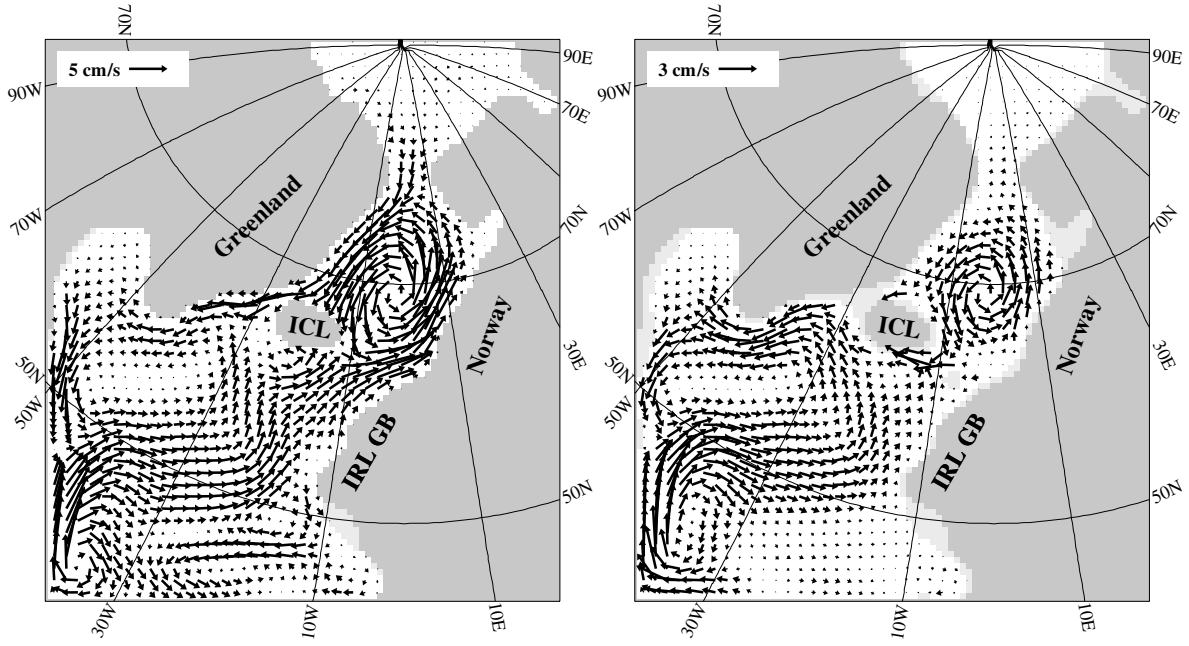

Fig. 13: Experiment R2, horizontal velocities at (left) 75 m and 450 m depth (right)

cant heat transport beyond this latitude. Experiment R1 gives slightly higher heat transports than experiment R2 because the meridional overturning cell penetrates farther northward (Fig. 15, left).

Figure 17 details northward heat transport at 48° N in the global model for experiments GM and G1. In both glacial experiments, positive (truly northward) heat transport in the intermediate-to-deep layers decreases dramatically (by 0.3 PW), as may be expected. But because of the general slow-down of meridional overturning circulation, negative (southward) heat transport decreases by a comparable amount. This

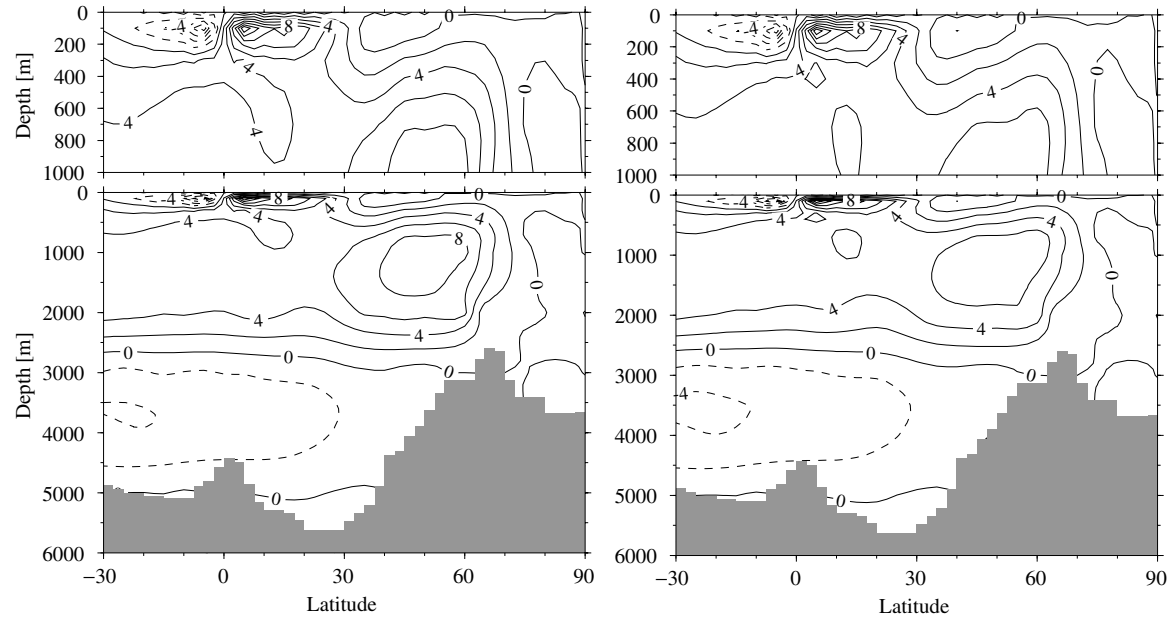

Fig. 14: Atlantic meridional overturning stream function from the global model, Sv. Left: 1:1-relation (G1) for SSS, right: 1 : 1.8-relation (G2)

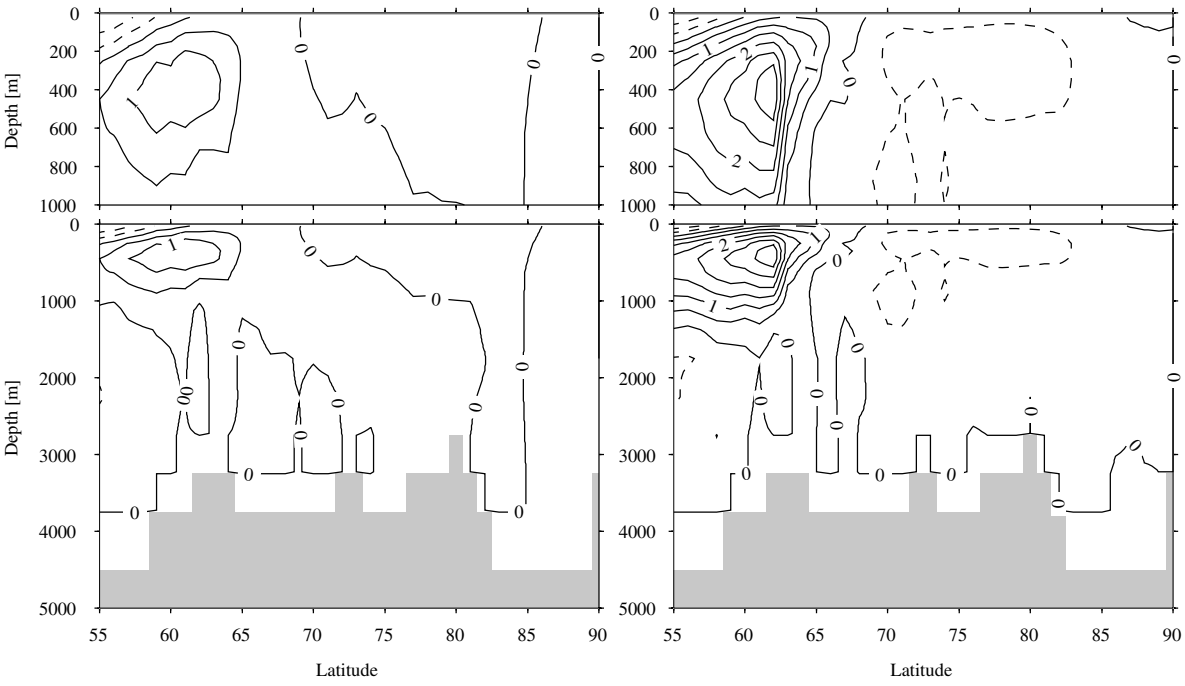

Fig. 15: Northern Atlantic meridional overturning stream function from the regional model, Sv. Left: 1 : 1-relation (R1), right: 1 : 1.8–2.8-relation (R2)

explains why the total heat delivered to the northern North Atlantic in experiment G1 diminishes from 0.35 PW to 0.25 PW by merely 0.1 PW (Fig. 16). In experiment G2 (not shown), this reduction is more pronounced because of the less vigorous meridional overturning cell.

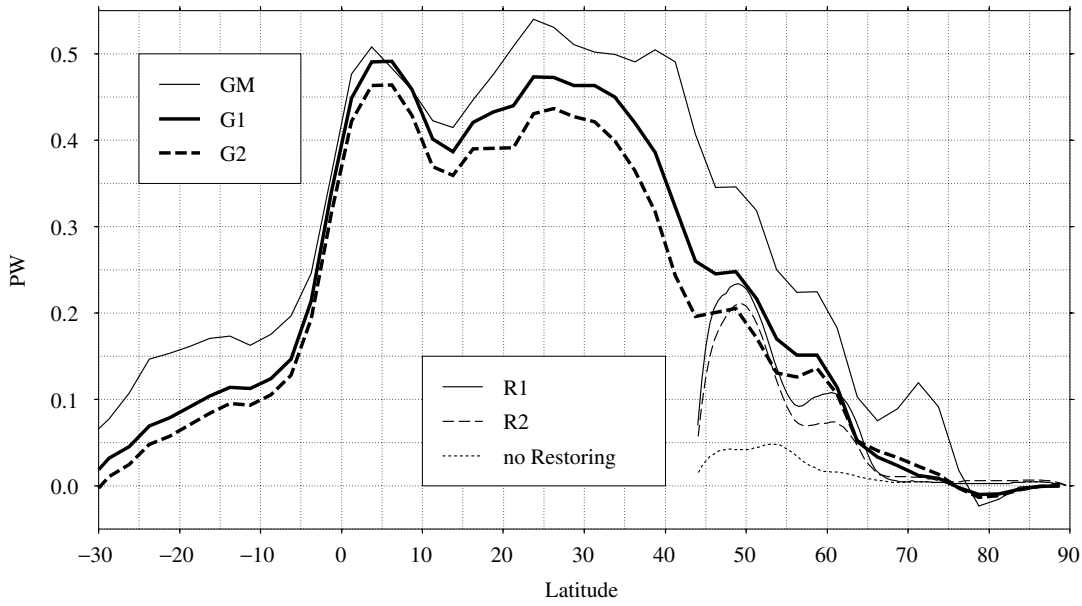

Fig. 16: Northward heat transports of global and regional experiments, PW. The dotted line indicates heat transport of R1 without restoring

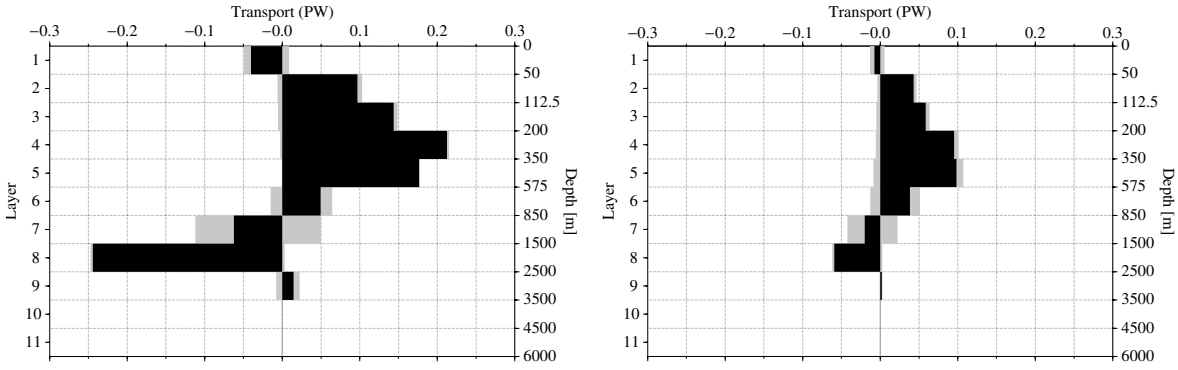

Fig. 17: North- and southward heat transports of experiments GM (left) and G1 (right) at 48° N versus depth, PW. Grey: northward and southward transport components, black: total

For comparison, experiment R2 was repeated without restoring to the global model results. The circulation pattern did not change considerably (not shown here), except for the restoring zones and their ultimate vicinity. This is illustrated by Figures 12 and 13: both regional LGM experiments are restored to quite similar temperatures and salinities at the southwestern boundaries, but nevertheless, GNS current velocities and overflow intensities differ drastically. Thus, these differences must be attributed to altered SSS forcing. The flow paths do not change very much under altered surface conditions, and it can be concluded that they are predominantly governed by topographic features. However, without lateral boundary restoring, the model cannot maintain the appropriate three-dimensional T and S distributions in its southwestern part, and T/S gradients are diminished by advection and diffusion. In consequence, (almost) the same currents transport different temperatures, and northward heat transport decreases by a factor of four (Fig. 16, dotted line).

Meridional Temperature Distribution

In experiments G1 and G2, global annual mean temperatures are lower by more than 2 °C and global annual mean salinities are approximately 1.2 units higher than in experiment GM (see Table 3). The an-

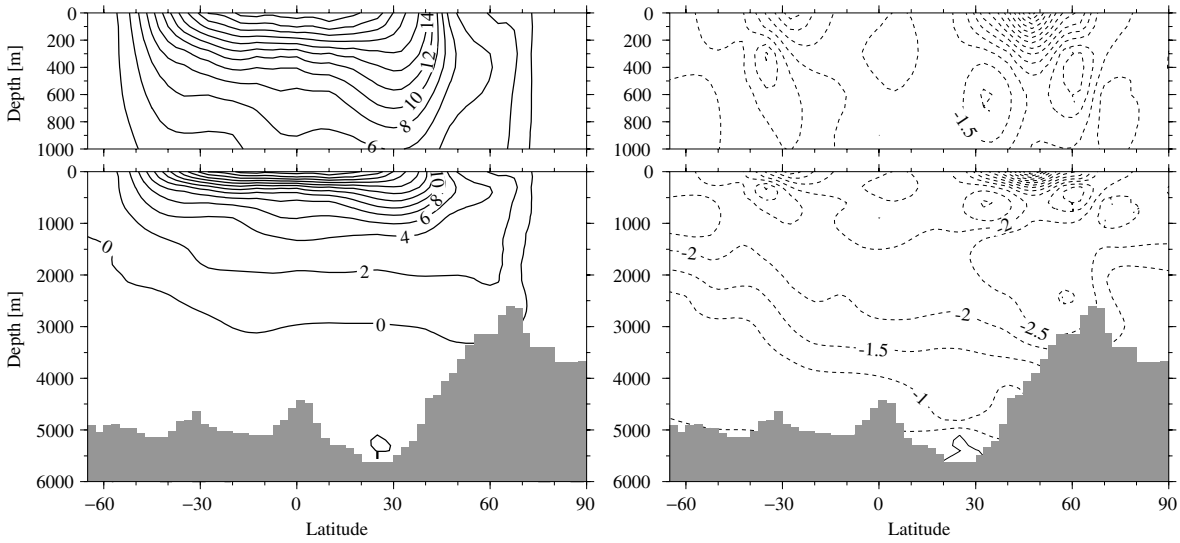

Fig. 18: Meridional temperature distribution along the GEOSECS transect for the global LGM experiment with 1 : 1-relation (G1), °C. Left: temperature, right: temperature difference G1 minus GM

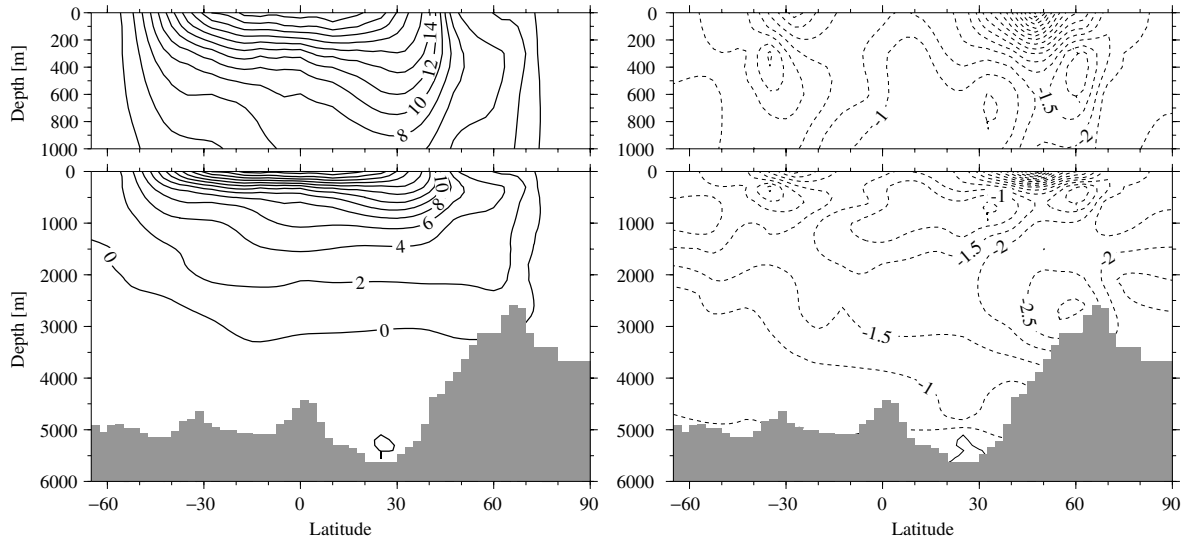

Fig. 19: Meridional temperature distribution along the GEOSECS transect for the global LGM experiment with 1 : 1.8-relation (G2), °C. Left: temperature, right: temperature difference G2 minus GM

nual mean temperature and salinity anomalies in the Atlantic Ocean are of a similar magnitude. Accordingly, temperature sections (Figs. 18 and 19) show a marked cooling, with a maximum of 8 °C near the surface of the North Atlantic. AABW is approximately 1 °C colder than in experiment GM. At the same time NADW is approximately 2 °C colder and does not sink as deep, as is indicated by the 2 °C isotherm in experiments G1 and G2 as compared to the 4 °C isotherm in experiment GM. The cooling of NADW is 0.5 °C larger in experiment G1 than in experiment G2.

The general cooling of deep and bottom waters is also evident from Figure 20. Upon entering the Argentine Basin at 4000 m depth, the temperature of AABW is approximately −1.2 to −1.3 °C and its salinity is 35.86. The change in salinity of AABW is approximately 1.4 units and therefore larger than the change in global mean salinity by 0.2 units. Consequently, similar to the temperature contrast, the salinity contrast be-

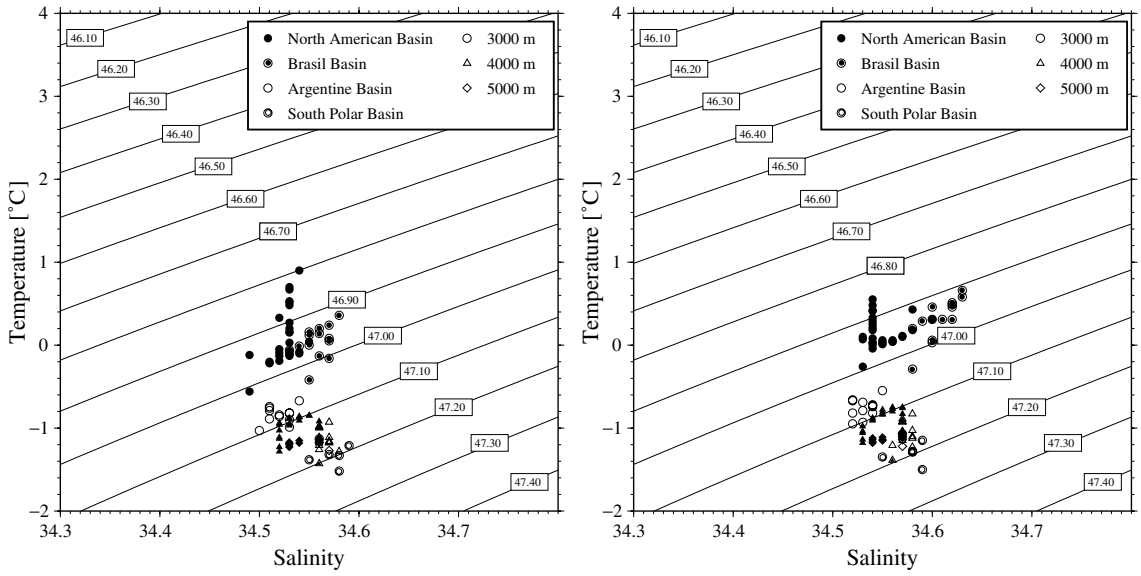

Fig. 20: Relationship between potential temperature and salinity in the Western Atlantic Trough. Left: experiment G1, right: experiment G2. Temperature, depth, and latitude ranges are the same as in Figure 7, but salinity and σ_4 ranges differ

tween NADW and AABW is reduced. Hence, the deep and bottom layers of the Atlantic Ocean are less stratified in experiments G1 and G2 than in experiment GM, which could also be interpreted as a lowering of the water-mass boundary between NADW and AABW (by less than 1000 m, which is the vertical resolution at this depth).

The 2.0 to 2.5 °C cooling of NADW is consistent with changes in benthic foraminiferal $\delta^{18}O$ and an ice-volume effect of 1.2 per mill, but smaller than the 4 °C cooling derived from pore fluids (Schrag et al. 1996). The higher density of AABW is maintained by an increase of salinity relative to NADW, in accordance with the scenario most favored by Zahn and Mix (1991). In the global model, this increase in bottom water salinity can be traced back to the glacial salinity anomaly imposed on Weddell Sea surface waters, which is based on SSS reconstructions by Melles (1991). The higher salinity of Antarctic surface and bottom waters may result from more intense sea-ice freezing.

The global mean salinity anomaly is higher than inferred from sea-level change by approximately 0.2 units. Additional experiments which parallel experiments G1 and G2, but in which a constant value of 0.2 units was subtracted from the SSS forcing fields, yielded a global mean salinity anomaly of 1.0 units with no visible change in meridional overturning or meridional temperature and salinity distributions.

In an extension of the LSG results, Figure 21 shows the vertical temperature sections along the GEOSECS transect from the regional model. Unlike the global model study, in which the Nordic Seas are filled entirely by a water mass with $T < 0$ °C, the regional model produces a tongue of warmer waters around 2–3 °C which penetrates the GNS, sinking below the colder waters in the very north. Due to the lower SSS used for driving experiment R1, convection around 68° N is not as deep as in experiment R2. In experiment R1 (left), convection stops at approximately 1500 m depth (3 °C isoline), whereas it reaches the bottom in experiment R2 (right) and spreads a relatively warm water mass with T ~ 4 °C all over the lower 3000 m of the GNS and the Arctic. (The actual convection "chimneys" cannot be seen in Figure 21 because convection takes place at approximately 68° N/0° E, i.e., slightly southeast of the transect – see Sarnthein et al. this volume, Fig. 12b). This is approximately 3–4 °C warmer than today, a tremendous present-to-glacial warming of the deep Nordic Seas, pointing to the perhaps worst consequence of taking summer-only reconstructions as representative of the entire glacial. High SST's reconstructed from the sediment cores and high glacial $\delta^{18}O$ values yield high surface salinities as well. Accordingly, the model generates very deep convection, thus mixing high SST values down to great depths. Apart from the unrealistic SSS gradients discussed above, the SSS values are also too high to realistically model the glacial high latitudes. With the omission of the seasonal cycle, $^{16}O/^{18}O$ fractionation due to freezing and melting sea ice (Stain and Tan 1993) is neglected as

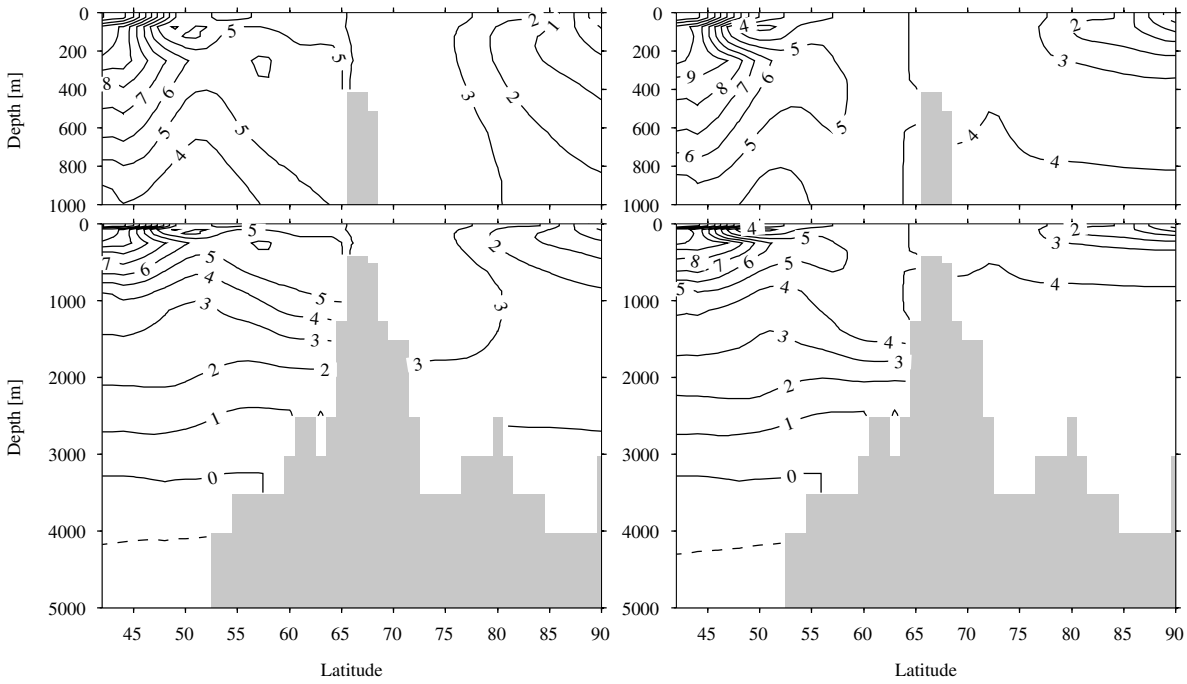

Fig. 21: Meridional temperature distribution along the GEOSECS transect for the regional LGM experiments R1 (left) and R2 (right), °C

well. Rohling and Bigg (1998) have shown that melting ice turns the linear $\delta^{18}O$:SSS relation into a nonlinear relation, such that high $\delta^{18}O$ values are linked to lower salinities. Now, the foraminifers which recorded glacial $\delta^{18}O$ most likely grew during phases of seasonal ice retreat, and, as a consequence, $\delta^{18}O$ values are presumably biased to higher values by this fractionation effect, making salinities computed by the approach used here too high. Any future attempt to model the glacial (sub-) arctic must carefully incorporate estimates of seasonal ice variations.

Conclusions

The following conclusions can be drawn from these global and regional model results:

- With regard to flow patterns between the northeastern Atlantic and the Nordic Seas, the glacial state was not very different from the present-day state: A near-surface inflow between Iceland and Scotland was balanced by deeper outflows and an East Greenland Current.
- Overall flow strength was diminished in the glacial state: The export of NADW to the Southern Ocean was reduced by 50 %. Consequently, in the North Atlantic the Gulf Stream was weakened, while in the South Atlantic, the North Brazil Current was weakened and the South Equatorial Current and Brazil Current were strengthened, which caused a net decrease in cross-equatorial heat transport of 0.1 PW.
- In the global LGM experiments, Atlantic deep waters cooled by 2 to 2.5 °C, while Atlantic bottom waters cooled by approximately 1 °C and maintained their higher density through a relative increase in salinity. This may be traced to the glacial salinity anomaly imposed on Weddell Sea surface waters, which was based on SSS reconstructions by Melles (1991) and may be explained by more intense sea-ice freezing.
- The representation of water masses as well as the determination of circulation and water-mass boundaries would likely profit from a higher vertical resolution in the global as well as in the regional model.
- The omission of the seasonal cycle and its sea-ice variation in the regional model causes the reconstruction of too high sea-surface salinities in the high northern latitudes and, therefore, an unrealistic glacial warming of the deep Nordic Seas in contrast to the global model.
- Integral measures of Atlantic circulation such as meridional overturning circulation and northward heat transport prove to be quite robust against the background of local uncertainties in SST and SSS reconstructions.

• Regarding the high latitudes of the North Atlantic, that is, the GNS and their neighboring basins, topography and reconstructed surface forcing fields play the most important role for flow patterns and current velocities. Lateral boundary restoring is less important, at least if the boundaries are far enough from the region of interest.
• Unlike flow patterns, three-dimensional temperature and salinity distributions are much more dependent on lateral restoring, which is equivalently valid for the transports of heat and salt.
• None of the two extreme $\delta^{18}O$: SSS ratios employed here seem to be an appropriate assumption for the glacial Atlantic. 1 : 1 gives too weak SSS gradients in the Nordic Seas. This may be partly caused by the omission of local variations. 1 : 1.8–2.8 yields similar gradients for the North Atlantic and Nordic Seas which are too strong.
• Neither coarse- or fine-resolution modeling alone is appropriate for assessing paleoclimatic reconstructions from sediment cores. The global model is relatively insensitive to small-scale, but nonetheless substantial, changes in reconstructed SSS, and is hence only of limited use for discrimination against specific reconstructions or transfer equations. On the contrary – and naturally – the regional model is very sensitive to even minor changes in the forcing data sets. However, it fails to reproduce important aspects of the paleoceanographic scenario, such as high-latitude heat transports, when it is not linked to global model results. Unfortunately, for the South Atlantic no high-resolution regional model has been developed. Thus, the combined global-regional work has not been extended to this region, and the densely spaced SST data which have been reconstructed within the Sonderforschungsbereich 261 at the University of Bremen have not been utilized yet.

Acknowledgments

Christian Schäfer-Neth thanks his colleagues at SFB 313 and the Institute of Geosciences for more than 7 years of continuous collaboration and efforts in reconstructing the data paleomodeling base. Special thanks to Michael Schulz for many fruitful discussions.

In addition, André Paul thanks Ernst Maier-Reimer, Uwe Mikolajewicz and Michael Lautenschlager for providing a copy of the Hamburg Large-Scale Geostrophic (LSG) ocean model. Furthermore, the authors are grateful to Dan Seidov for many useful discussions regarding the numerical modeling of the ocean circulation at the LGM.

Most of this research was funded by the Deutsche Forschungsgemeinschaft: The authors were supported by the Sonderforschungsbereich 313 (Project B4) at the University of Kiel and Sonderforschungsbereich 261 (Project C2, Contribution No. 285) at the University of Bremen.

Parts of this research were conducted at the Scripps Institution of Oceanography, La Jolla, California, USA, and were funded by the Alexander von Humboldt Foundation (through a Feodor Lynen Research Fellowship) and the California Space Institute.

The authors gratefully acknowledge the constructive comments of an anonymous reviewer which helped to considerably improve the manuscript.

References

Bryan, K., and L. J. Lewis, A water mass model of the world ocean circulation, *J. Geophys. Res.*, 84, 2503–2517, 1979.

CLIMAP Project Members, Seasonal reconstructions of the Earth's surface at the Last Glacial Maximum, *Geol. Soc. Am. Map and Chart Ser.*, MC-36, 1981.

Danabasoglu, G., and J. C. McWilliams, Sensitivity of the global ocean circulation to parameterizations of mesoscale tracer transports, *J. Clim.*, 8, 2967–2987, 1995.

Dietrich, G., *Atlas of the hydrography of the northern North Atlantic ocean*, 140 pp., Conseil International pour l'Exploration de la Mer, Service Hydrographique, Charlottenlund Slot, Denmark, 1969.

Duplessy, J. - C., L. Labeyrie, A. Juillet-Leclerc, F. Maitre, J. Duprat, and M. Sarnthein, Surface salinity reconstruction of the North Atlantic Ocean during the last glacial maximum, *Oceanol. Acta*, 14, 311–324, 1991.

ETOPO5, *Digital relief of the surface of the Earth*, National Geophys. Data Center, Boulder, Colorado, 1986.

Epstein, S., R. Buchsbaum, H. A. Lowenstam, and H. C. Urey, Revised carbonate-water isotopic temperature scale, *Geol. Soc. Am. Bull.*, 64, 1315–1325, 1953.

Fairbanks, R. G., A 17000-year glacio-eustatic sea level record: Influence of glacial melting rates on the Younger Dryas event and deep-ocean circulation, *Nature*, 342, 637–642, 1989.

Farrow, D. E., and D. P. Stevens, A new tracer advection scheme for Bryan and Cox type ocean general circulation models, *J. Phys. Oceanogr.*, 25, 1731–1741, 1995.

Fichefet, T., S. Hovine, and J. - C. Duplessy, A model study of the Atlantic thermohaline circulation during the Last Glacial Maximum, *Nature*, 372, 252–255, 1994.

GEOSECS, Atlantic, Pacific, and Indian Ocean expeditions: Shore-based data and graphics, in *GEOSECS Executive Committee*, edited by H G. Östlund, H. Craig, W. S. Broecker, and D. Spencer, I.D.O.E., National Science Foundation, 7, 1987.

Haupt, B. J., C. Schäfer-Neth, and K. Stattegger, Modelling sediment drifts; A coupled oceanic circulation-sedimentation model of the northern North Atlantic, *Paleoceanogr.*, 9, 897–916, 1994.

Haupt, B. J., C. Schäfer-Neth, and K. Stattegger, Three-dimensional numerical modelling of Late Quaternary paleoceanography and sedimentation in the northern North Atlantic, *Geol. Rundsch.*, 84, 137–150, 1995.

Hellerman, S., and M. Rosenstein, Normal monthly mean wind stress over the world ocean with error estimates, *J. Phys. Oceanogr.*, 13, 1093–1104, 1983.

Herterich, K., S. Determann, B. Grieger, I. Hansen, P. Helbig, S. Lorenz, A. Manschke, M. Matthies, A. Paul, R. Schlotte, and U. Wyputta, Reconstructing and modelling the Last Glacial Maximum: Beyond CLIMAP, in *Use of Proxies in Paleoceanography: Examples from the South Atlantic*, edited by G. Fischer, and G. Wefer, Springer, Heidelberg, 687–714, 1999.

Hoffmann, G., Stabile Wasserisotope im allgemeinen Zirkulationsmodell ECHAM, Ph.D. dissertation No. 27, Max-Planck-Institut für Meteorologie, Hamburg, Germany, 98 pp., 1995.

Johns, T. C., R. E. Carnell, J. F. Crossley, J. M. Gregory, J. F. B. Mitchell, C. A. Senior, S. F. B. Tett, and R. A. Wood, The second Hadley Centre coupled ocean-atmosphere GCM: model description, spinup and validation, *Clim. Dyn.*, 13, 103–134, 1997.

Joussaume, S., and J. Jouzel, Paleoclimatic tracers: An investigation using an atmospheric general circulation model under ice age conditions. 2. Water isotopes, *J. Geophys. Res.*, 98, 2807–2830, 1993.

Knauss, J., A note on the transport of the Gulf Stream, *Deep Sea Res.*, 16, suppl., 117–124, 1969.

Large, W. G., G. Danabasoglu, S. C. Doney, and J. C. McWilliams, Sensitivity to surface forcing and boundary layer mixing in a global ocean model: Annual mean climatology, *J. Phys. Oceanogr.*, 27, 2418–2447, 1997.

Larsen, J. C., Transport and heat flux of the Florida Current at 27° N derived from cross-stream voltages and profiling data: Theory and observations, *Philos. Trans. Royal Soc. London A*, 338, 169–236, 1992.

Lehman, S. J., G. A. Jones, L. D. Keigwin, E. S. Andersen, G. Butenko, and S. - R. Østmo, Initiation of Fennoscandian ice-sheet retreat during the last deglaciation, *Nature*, 349, 513–516, 1991.

Levitus S., Climatological atlas of the world ocean, *NOAA Prof. Pap.*, 14, US Govt. Print. Off., Washington, 1982.

Levitus S., and T. P. Boyer, World Ocean Atlas 1994 Volume 4: Temperature, *NOAA Atlas NESDIS*, 4, 117 pp., 1994.

Levitus S., R. Burgett, and T. P. Boyer, World Ocean Atlas 1994 Volume 3: Salinity, *NOAA Atlas NESDIS*, 3, 99 pp., 1994.

Leonard, B. P., A stable and accurate convective modeling procedure based on quadratic upstream interpolation, *Computer Methods in Applied Mechanics and Engineering*, 19, 59–98, North-Holland Publ. Co, 1979.

Lorenz, S., B. Grieger, P. Helbig, and K. Herterich, Investigating the sensitivity of the atmospheric general circulation model ECHAM 3 to paleoclimatic boundary conditions, *Geol. Rundsch.*, 85, 513–524, 1996.

Macdonald, A. M., The global ocean circulation: a hydrographic estimate and regional analysis, *Progr. Oceanogr.*, 41, 281–382, 1998.

Marotzke, J., Influence of convective adjustment on the stability of the thermohaline circulation, *J. Phys. Oceanogr.*, 21, 903–907, 1991.

Maier-Reimer, E., U. Mikolajewicz, and K. Hasselmann, Mean circulation of the LSG OGCM and its sensitivity to the thermohaline surface forcing, *J. Phys. Oceanogr.*, 23, 731–757, 1993.

Melles, M., Late Quaternary paleoglaciology and paleoceanography at the continental margin of the southern Weddell Sea, Antarctica, *Berichte zur Polarforschung*, 81, Alfred-Wegener-Institut für Polar- und Meeresforschung, 1991.

Mienert, J., J. T. Andrews, and J. D. Milliman, The East Greenland continental margin (65° N) since the last deglaciation: Changes in seafloor properties and ocean circulation, *Mar. Geol.*, 106, 217–238, 1992.

Pacanowski, R., K. D. Dixon, and A. Rosati, The G.F.D.L Modular Ocean Model Users Guide, *GFDL Ocean Group Technical Report No. 2*, Geophys. Fluid Dynamics Laboratory / NOAA, Princeton University, 1993.

Paul, A., S. Mulitza, J. Pätzold, and T. Wolff, Simulation of oxygen isotopes in a global ocean model, in *Use of Proxies in Paleoceanography: Examples*

from the South Atlantic, edited by G. Fischer, and G. Wefer, Springer, Heidelberg, 655–686, 1999.

Rahmstorf, S., A fast and complete convection scheme for ocean models, in *MOM 2. Documentation, User's Guide and Reference Manual*, edited by R. C. Pacanowski, 329 pp., GFDL Ocean Group, Tech. Rep. 3.2, GFDL, Princeton, New Jersey, 1996.

Rohling E. J., and G. R. Bigg, Paleosalinity and $\delta^{18}O$; A critical assessment, *J. Geophys. Res.*, 103, 1307–1318, 1998.

Sarnthein, M., K. Stattegger, D. Dreger, H. Erlenkeuser, P. Grootes, B. J. Haupt, S. Jung, T. Kiefer, W. Kuhnt, U. Pflaumann, C. Schäfer-Neth, H. Schulz, M. Schulz, D. Seidov, J. Simstich, S. van Kreveld, E. Vogelsang, A. Völker, and M. Weinelt, Fundamental modes and abrupt changes in North Atlantic circulation and climate over the last 60 ky – Concepts, reconstruction and numerical modeling, this volume.

Schäfer-Neth, C., Changes in the seawater salinity-oxygen isotope relation between Last Glacial and present: Sediment core data and OGCM modelling, *Paleoclim.*, 2 (2–3), 101–131, 1998.

Schäfer-Neth, C., and K. Stattegger, Meltwater pulses in the northern North Atlantic: Retrodiction and forecast by numerical modelling, *Geol. Rundsch.*, 86, 492–498, 1997.

Schäfer-Neth, C., and K. Stattegger, Icebergs in the North Atlantic: Modelling circulation changes and glacio-marine deposition, in *Modeling of Sedimentary Systems*, edited by J. Harff, and K. Stattegger, Springer, Heidelberg, 63–78, 1999.

Schmidt, G., Oxygen-18 variations in a global ocean model, *Geophys. Res. Lett.*, 25, 1201–1204, 1998.

Schmitz Jr., W. J., On the interbasin-scale thermohaline circulation, *Rev. of Geoph.*, 33, 151–173, 1995.

Schrag, D. P., G. Hampt, and D. W. Murray, Pore Fluid Constraints on the Temperature and Oxygen Isotopic Composition of the Glacial Ocean, *Nature*, 272, 1930–1932, 1996.

Schulz, H., Meeresoberflächentemperaturen im Nordatlantik und in der Norwegisch-Grönländischen See vor 9 000 Jahren. Auswirkungen des frühholozänen Insolationsmaximums, Ph.D. dissertation, University of Kiel, Germany, 119 pp., 1994.

Seidov, D., and R. Prien, A coarse resolution North Atlantic ocean circulation model: An intercomparison study with a paleoceanographic example, *Ann. Geoph.*, 14, 246–257, 1996.

Seidov, D., M. Sarnthein, K. Stattegger, R. Prien, and M. Weinelt, North Atlantic ocean circulation during the Last Glacial Maximum and a subsequent meltwater event: A numerical model, *J. Geophys. Res.*, 101, 16305–16332, 1996.

Shackleton, N. J., Attainment of isotopic equilibrium between ocean water and the benthonic foraminifera uvigerina: Isotopic changes in the ocean during the Last Glacial, Centre National de la Recherche Scientifique, Paris, France, *Colloque CNRS*, 219, 203–210, 1974.

Shea, D. J., K. E. Trenberth, and R. W. Reynolds, A global monthly sea surface temperature climatology, *NCAR Technical Note NCAR/TN-345*, NCAR, Boulder, Colorado, 167 pp., 1990.

Simstich, J., Die ozeanische Deckschicht des Europäischen Nordmeers im Abbild stabiler Isotope von Kalkgehäusen unterschiedlicher Planktonforaminiferenarten, Ph.D. dissertation, University of Kiel, Germany, 96 pp., 1999.

Strain, P. M., and F. C. Tan, Seasonal evolution of oxygen isotope-salinity relationships in high-latitude waters, *J. Geophys. Res.*, 98, 14,589–14,598, 1993.

Vogelsang, E., Paläo-Ozeanographie des Europäischen Nordmeers an Hand stabiler Kohlenstoff- und Sauerstoffisotopen, Ph.D. dissertation, University of Kiel, Germany, 136 pp., 1990.

Wadhams, P., The Ice Cover, in *The Nordic Seas*, edited by B. G. Hurdle, pp. 21–87, Springer, Heidelberg, 1986.

Wang, L., M. Sarnthein, J. - C. Duplessy, H. Erlenkeuser, S. Jung, and U. Pflaumann, Paleo sea surface salinities in the low-latitude Atlantic: The $\delta^{18}O$ Record of Globigerinoides ruber (white), *Paleoceanogr.*, 10, 749–761, 1995.

Weaver, A. J., and T. M. C. Hughes, On the incompatibility of ocean and atmosphere models and the need for flux adjustments, *Clim. Dyn.*, 12, 141–170, 1996.

Weinelt, M., Veränderungen der Oberflächenzirkulation im Europäischen Nordmeer während der letzten 60.000 Jahre – Hinweise aus stabilen Isotopen, Ph.D. dissertation, University of Kiel, Germany, 106 pp., 1993.

Weinelt, M., M. Sarnthein, U. Pflaumann, H. Schulz, S. Jung, and H. Erlenkeuser, Ice-Free Nordic seas during the Last Glacial Maximum? Potential sites of deepwater formation, *Paleoclim.*, 1, 283-309, 1996.

Winguth, A. M. E., D. Archer, E. Maier-Reimer, U. Mikolajewicz, and J. - C. Duplessy, Sensitivity of paleonutrient tracer distributions and deep sea circulation to glacial boundary conditions, *Paleoceanogr.*, 14, 304–323, 1998.

Wüst, G., Das Bodenwasser und die Gliederung der Atlantischen Tiefsee, *Wiss. Ergeb. Deutsch. Atlant. Exped. "Meteor", 1925–1927, Bd. VI, Teil 1, Schich-*

tung und Zirkulation des Atlantischen Ozeans, 1. Lief., 1933.

Wüst, G., Die Stratosphäre des Atlantischen Ozeans, *Wiss. Ergeb. Deutsch. Atlant. Exped. "Meteor", 1925–1927, Bd. VI, Teil 1, Schichtung und Zirkulation des Atlantischen Ozeans, 2. Lief.*, 1935.

Wüst, G., Stromgeschwindigkeiten und Strommengen in den Tiefen des Atlantischen Ozeans, *Wiss. Ergeb. Deutsch. Atlant. Exped. "Meteor", 1925–1927, Bd. VI, Teil 2, Quantitative Untersuchungen zur Statik und Dynamik des Atlantischen Ozeans, 6. Lief.*, 1957.